Development and characterization of an airborne-based instrument used to measure nitric acid during the NASA TRACE-P field experiment

Mark A. Zondlo[1,2*], R. Leon Mauldin[1], Ed Kosciuch[1], Christopher A. Cantrell[1], and Fred L. Eisele[1]

[1]Atmospheric Chemistry Division and [2]Advanced Study Program
1850 Table Mesa Dr.
P.O. Box 3000
National Center for Atmospheric Research
Boulder, Colorado, 80305

Submitted to *Journal of Geophysical Research – Atmospheres*
Special Section on NASA TRACE-P

Index terms
Primary: 0394 instruments and techniques
Secondary: 0365, troposphere – composition and chemistry; 0305, aerosols and particles

* To whom correspondence should be addressed:
Mark Zondlo
Southwest Sciences, Inc.
1570 Pacheco Street, Suite E-11
Santa Fe, NM 87505
Phone: (505) 984-1322
Fax: (505) 988-9230
e-mail: mzondlo@swsciences.com

Running title: Nitric acid instrument in TRACE-P

11/27/02

Abstract. A new inlet and instrument have been developed for the rapid measurement of gas phase nitric acid (HNO_3) from an airborne platform. The inlet was kept near ambient temperatures with a very short sampling time (100 ms) to minimize desorption of particle nitrates. In addition, inlet surface adsorption problems were minimized by the use of extruded perfluoro-alkoxy (PFA) as a sampling material. Nitric acid was detected by selected ion chemical ionization mass spectrometry using deprontonated methanesulfonic acid as a reagent ion. Laboratory tests showed no interferences from NO, NO_2, NO_3, and N_2O_5 under wet (RH=100%) or dry (RH=0%) conditions at levels exceeding those found in the troposphere. Nitric acid was measured every 5 s for a 3 s integration period with a limit of detection of 5 pptv. Absolute uncertainties including systematic errors are the limit of detection (5 pptv) plus ± 15% for HNO_3 > 200 pptv, ± 20% for HNO_3 100-200 pptv, and ± 25% for HNO_3 < 100 pptv (± 2σ). The instrument was calibrated by the addition of isotopically-labeled $H^{15}NO_3$ near the front of the ion source on a continual basis. The inlet and instrument were flown on the NASA P-3B airplane as part of the NASA TRACE-P field campaign off the coast of Asia in February-April 2001. Rapid changes in ambient HNO_3 were resolved, suggesting minimal influences from instrument surfaces. Finally, the measurements compared favorably with the University of New Hampshire's mist chamber/ion chromatography instrument flown onboard the NASA DC-8 aircraft during two intercomparison flights. The in-flight performance of the instrument is demonstrated under the wide range of conditions observed in TRACE-P.

Introduction

Nitric acid, HNO_3, plays important roles in both the gas phase and condensed phase chemistry of the troposphere. Gas phase HNO_3 is formed by the oxidation of the nitrogen oxides NO and NO_2 (NO_x), species that play important roles in ozone photochemistry. Tropospheric HNO_3 has a relatively long lifetime with respect to photolysis (weeks) and reaction with OH (weeks). The dominant loss mechanism is by removal onto particle surfaces, followed by either wet or dry deposition, with a heterogeneous lifetime of a few days [*Liang et al., 1998*]. In the condensed phase, HNO_3 usually dissociates into particulate nitrate, NO_3^-. The availability of gas phase HNO_3 has been shown to be important in liquid particle growth and composition [*Kerminen et al., 1997; Adams et al., 1999*]. Furthermore, HNO_3 uptake by particles indirectly affects cirrus cloud properties by altering the deliquescence behavior of salt particles [*Lin and Tabazadeh, 2002*] and by activating cloud condensation nuclei [*Laaksonen et al., 1997*]. Modeling studies suggest that gas phase HNO_3 assists in the development of unhealthy particulate matter in urban areas [*Meng et al., 1997*]. Because of the role of HNO_3 as a sink for NO_x and its significance to aerosol particle dynamics, the chemistry of HNO_3 is important towards understanding issues such as photochemical smog, acid deposition, climate change, and human health.

Numerous modeling and field studies have investigated the tropospheric chemistry of HNO_3, and model results, though improving, can significantly differ from the measurements [*Singh et al., 1996; Jacob et al., 1996; Singh et al., 1998*]. One of the major uncertainties of HNO_3 is the partitioning between the gas and condensed phases [*Dentener et al., 1996; Adams et al., 1999*]. Based on laboratory and modeling studies, a number of atmospheric surfaces have been implicated in removing gas phase HNO_3, but in-situ verification of these heterogeneous processes is lacking [*Dentener et al., 1996; Zondlo et al., 1997; Abbatt, 1997; Underwood et al.,*

2001]. Nonetheless, particulate nitrates are thought to be a significant component of aerosol mass, especially downwind of urban and agricultural areas [*Adams et al., 1999*].

Understanding the chemistry of HNO_3 has been further complicated by the numerous challenges in its measurement, especially on airborne platforms where conditions change rapidly. Resolving HNO_3 concentrations in thin layers of particles, for example, requires an instrument with high sensitivity and short integration times. Furthermore, instrument surfaces should have minimal influence on the sampling of the ambient air. Otherwise, rapid changes in gas phase HNO_3 are buffered by adsorption/desorption of HNO_3 on instrument and inlet surfaces, and thus the measurements lose their time response. One method used to minimize surface effects is by heating the inlet surfaces [*Neuman et al., 2000; 2002*]. However, heating induces the possibility that particulate nitrate may desorb into gas phase HNO_3 and thereby result in artificially inflated gas phase HNO_3 measurements. Thus, the characteristics of an ideal HNO_3 instrument for aircraft studies are high sensitivity and temporal resolution, short sampling times, inlet surfaces with minimal adsorption problems, and inlets kept as close to ambient conditions as possible.

The mist chamber/ion chromatography technique [*Talbot et al., 1997; Talbot et al., 1999*] has been used extensively on aircraft for measuring HNO_3 as well as a variety of other soluble compounds simultaneously. Briefly, ambient air is pulled into the cabin at very high flow rates (1500-3000 sLpm) and collected on a fine particle mist. The corresponding solutions are analyzed by ion chromatography. The technique is extremely reliable and sensitive (3 pptv) but has relatively long integration periods (minutes) for aircraft platforms. Furthermore, because particles less than ~ 2.5 μm in aerodynamic diameter are sampled by the inlet, fine nitrate-containing aerosols may complicate the gas phase measurements.

Airborne chemical ionization mass spectrometer (CIMS) instruments have shown high time resolution (< 1 Hz) with excellent sensitivity (> 1 count $pptv^{-1}$ s^{-1}) and selectivity. *Neuman*

et al. [2000, 2002] use SiF_5^- ion chemistry which is extremely sensitive (1.1 ion counts $pptv^{-1}$ s^{-1}) and fast (≤ 1 Hz), but their use of heated PFA inlets at 50º C may complicate the distinction between particulate and gas phase HNO_3, particularly in polluted areas. *Arnold et al.* [1992], *Reiner et al.* [1998], *Schneider et al.* [1998] and *Miller et al.* [2000] use ion chemistry, $CO_3^-(H_2O)$, that has the potential for interferences at the pressures of the lower and middle troposphere [*Möhler and Arnold, 1991*], and their stainless steel inlets remain well above ambient temperatures. To acquire accurate budgets of HNO_3, unambiguous measurements of gas phase HNO_3 need to be made near ambient conditions and at high-temporal resolutions.

To this end, a new inlet and CIMS instrument design has been developed and characterized to measure HNO_3 from an airborne platform. The instrument used deprotonated methanesulfonic acid ($CH_3SO_3^-$, MSA) as a reagent ion for HNO_3 detection and a unique choice of inlet design and materials for the sampling of the ambient airstream. The instrument was flown on the NASA P-3B aircraft as part of the NASA Transport and Chemical Evolution over the Pacific (TRACE-P) field experiment off the coast of eastern Asia in February-April 2001. Results from the field and in the laboratory suggest that the technique has a low limit of detection (5 pptv) and a fast time response (5 s). A description of the behavior and characteristics of the instrument under a wide variety of laboratory and field conditions is presented.

Experimental

The detection of HNO_3 was conducted using selected ion chemical ionization mass spectrometry with deprotonated methanesulfonic acid (MSA) as the reagent ion. The instrument was part of a four channel mass spectrometer system also containing components to measure hydroxyl radicals (OH), gas phase sulfuric acid (H_2SO_4), and gas phase MSA [*Mauldin et al.,*

1999], and components for measuring peroxy radicals HO_2/RO_2 [*Cantrell et al., this issue*]. Each channel had independent ionization schemes, flow controls, pressure controls, electrostatic lenses, quadrupoles, and electron multipliers, but they shared a common vacuum housing inside the aircraft. The vacuum housing was pumped by three 1000 L s^{-1} turbomolecular pumps in four stages. The first stage was pumped at a pressure of 10^{-2} Torr, the second stage of lenses and skimmers was pumped at 10^{-3} Torr, the quadrupoles were pumped at ~ 6 x 10^{-5} Torr, and the Channeltron electron multipliers in the last stage were at 3×10^{-5} Torr. The 4-channel system and corresponding inlets were located on the front, port side of the P3-B aircraft. Figure 1 shows a photo of the inlet and its location on the P3-B aircraft, and Figure 2 shows a schematic of the HNO_3 inlet and instrument. The inlet/instrument consisted of four parts: (1) a long, shrouded duct to straighten and slow the ambient airflow outside the plane, (2) a transport tube to bring the sampled air toward the airplane and for calibration, (3) an ion-molecule reaction region, and (4) the vacuum housing of ion lenses and quadrupoles inside the plane. For clarity, the general term "inlet" will refer to all parts of the instrument outside the airplane (1-3).

The shrouded duct (l=76.8 cm, 7.6 cm id, 8.9 cm od) was scaled down by a factor of 1.5 from the one described in *Eisele et al.* [1997]. The aluminum duct was tipped 9º away from the aircraft and secured at the back by an aluminum pylon that extended 15 cm from the fuselage of the aircraft (Fig. 1). The front, center of the duct was about 40 cm away from the aircraft surface, or about three times the distance that the boundary layer was calculated to expand out from the aircraft at this station. A shroud of 19.6 cm length (16.0 cm o.d., 13.3 cm i.d) had an elliptically-shaped surface to minimize turbulence effects while straightening, but not slowing, the airflow. The duct was concentric with the shroud, beginning 9.3 cm inside the shroud and continuing to the back of the pylon. The purpose of the duct was to transport the sampled air from a turbulence free region to the transport tube and to slow the flow by about an order of

magnitude relative to the free air speed (110-160 m s^{-1}) via a restricting orifice (r=1.9 cm) on the back end of the duct. Wind tunnel tests in *Eisele et al.* [1997] indicated that the airflow remained non-turbulent in the center of the duct at angles of attack less than 17°, and the scaled down version of inlet used here was expected to behave similarly.

A transport tube (2, Fig. 2), located about 65 cm downstream from the front of the duct, pulled a sample flow of 4-6 sLpm air toward the ion source region (3, Fig. 2). The transport tube (1.9 cm i.d., 2.2 cm o.d., l=10 cm), composed of extruded perfluoroalkoxy (PFA), was transverse to the duct, and its top was just below the centerline of the inner duct. The remainder of the flow in the duct (~ 10^4 sLpm depending upon air speed and ambient pressure) was vented out the back through the restricted opening. On the forward facing side of the transport tube, a semicircle notch of r=1 cm was cut out near the top, and a PFA cap covered the top of the transport tube. In this way, the air that entered the tube generally was pulled down toward the ion source. Because the transport tube extended to the middle of the duct, it was unavoidable that turbulence developed in the duct near and downstream of the transport tube. However, air sampled by the transport tube should have had minimal contact with the aluminum surfaces of the duct up to this location. As will be demonstrated later, observational data on the response of the inlet to changes in gas phase HNO_3 concentration support this assertion.

Air sampled into the transport tube under went an 81° deflection, and subsequent turbulence and contact with transport tube surfaces was unavoidable. Although cartridge heaters and an RTD temperature sensor were placed in the aluminum housing surrounding the transport tube, these heaters were never activated during flight and were only used to heat the inlet on-ground if necessary (e.g. for cleaning). Temperature readings indicated that the transport tube remained within 5 K of the ambient temperature during flight. Because the sampled air readily contacted the transport tube walls at near ambient temperatures and humidities, it was necessary

to find a material that was particularly inert to surface adsorption and desorption of HNO_3. *Neuman et al.* [1999] reported that PFA tubing was an optimal choice for inlet materials for HNO_3 sampling. However, even PFA had significant adsorption problems below 10ºC, and *Neuman et al.* [1999] concluded that inlets needed to be heated to at least this temperature.

A very similar inlet to the one described above was flown on the NSF NCAR C-130 as part of the Tropospheric Ozone Production about the Spring Equinox (TOPSE) field campaign from Feb.-May 2000 from Colorado northward to the Arctic Ocean. Although no robust HNO_3 measurements were made during this campaign due to numerous problems, significant advances were made in inlet design and characterization from in-flight tests. The inlet initially used regular (machined) PFA as a choice for a sampling tube with the finding of similar conclusions by *Neuman et al.* [1998]. In other words, whenever the inlet became even slightly cold, the response of the inlet to changes in gas phase HNO_3 was very slow (timescale of minutes for a factor of ten change in concentration). To help mitigate this problem, an extruded PFA tube replaced the machined PFA tube, and it showed excellent response, even under very cold conditions. Presumably, extruded PFA has significantly less surface area and is less porous than machined PFA, thereby giving far superior transmission of gas phase HNO_3 down the tube. Finally, it is important to note that the dimensions of the transport tube used in TRACE-P (1.9 cm in diameter and only ~ 10 cm long) also helped to minimize the available surface contact with ambient air.

Based on the C-130 flights in TOPSE and additional results from the laboratory, extruded PFA was the material of choice for the transport tube on the NASA P-3B aircraft. Therefore, the turbulence and temperature of the sampled air inside the transport tube were no longer a major concern. Three additional flows were added in the transport tube. First, about 3 cm below the top of the tube, a series of holes 1 mm in diameter encircled the circumference of the tube (not

shown in Figure 2 for clarity). These holes allowed for the addition of zero air into the top of the transport tube for examining the amount of HNO_3 adsorbed onto the inlet surfaces downstream of this point. A second hole about 5 cm down from the top of the transport tube allowed for the introduction of a 1.1 mm o.d., 0.6 mm i.d. tube to flow isotopically-labeled $H^{15}NO_3$ for calibration. Finally, a flow of aero air could be added to the ambient air at the end of the transport tube immediately before entering the ion source. This flow was most often used to examine for background signals of HNO_3 downstream from the transport tube.

The ambient air next passed through a removeable type 316 stainless steel tube (l=8.76 cm, id=1.22 cm, od=1.27 cm) to enter the ion source (3, Fig. 2). This tube, although relatively short, was composed of stainless steel in order to remain at ground potential (uncharged). A notched TFE collar around the outside of the stainless steel tube kept it secured in-flight and also served as the source of the reagent ion, methanesulfonic acid (MSA, CH_3SO_3H). MSA was physically applied to a 0.05 cm indentation in the TFE by rubbing a piece of PFA tubing dipped in MSA (J.T. Baker, 99.7%) to ensure a visual even distribution of small droplets. MSA was applied to the TFE collar before every flight, and the entire MSA assembly (TFE collar and s.s. tube) was manually placed into the ion source. Similarly, the MSA assembly was removed and cleaned immediately after flight to prevent MSA from significantly coating the surfaces of the ion source while on the ground. Any residual MSA on other parts of the ion source were removed by heating the entire ion source and transport tube while on the ground.

A flow of ~ 3 sLpm zero air, termed “sheath flow”, was distributed around the outside of the stainless steel tube through a showerhead assembly of 0.75 mm holes and fine mesh screens to minimize turbulence. The sheath flow passed over the TFE indentation and picked up MSA vapor. About 1 cm downstream of the MSA source, MSA vapor flowed over a 1.1 mC americium-241 source and was ionized through a multistep, charge transfer process:

$$^{241}Am \rightarrow \alpha \text{ particles} \rightarrow \rightarrow O_2^- \rightarrow \rightarrow MSA^-$$

The radioactive source was a 0.7 cm wide strip of americium-241 radioactive in the center of a 1.3 cm x 7.2 cm gold foil. The foil was positioned 0.5 cm behind the end of the stainless steel tube and held on the outside of a 2.28 cm diameter mount. In this way, alpha particles ionized only the sheath air on the outermost, annular layer, and direct ionization (and associated radical production) of the ambient airstream was prevented.

The flow of MSA and other ions joined the flow of the ambient air at the end of the stainless steel tube. Electrostatic lenses pushed the newly created ions toward the center of the ambient stream where ion-molecule reactions occurred through a drift region of 6 cm. Initial potentials were around -350 V, and average electric fields in this region were ~ 50 V cm^{-1}. The residence time of ions in the drift tube under typical flow conditions was ~ 50 ms, sufficient time for the ion-molecule species to achieve equilibrium. Nitric acid clustered with MSA in the following equilibrium:

$$HNO_3 + CH_3SO_3^- + M \leftrightarrow HNO_3 \bullet CH_3SO_3^- + M$$

By rearranging the equilibrium equation, the concentration of nitric acid was obtained:

$$[HNO_3] = \frac{[HNO_3 \bullet CH_3SO_3^-]}{c \cdot [CH_3SO_3^-]} \quad \begin{matrix} \leftarrow m/e\ 158 \\ \leftarrow m/e\ 95 \end{matrix}$$

where c is a constant calculated by adding a known amount of isotopically-labeled $H^{15}NO_3$ to the transport tube. In practice, the raw HNO_3 signal is the ratio of the ion counts at m/e 158 ($HNO_3 \bullet CH_3SO_3^-$) and at m/e 95 ($CH_3SO_3^-$). Regardless of the change of ion counts for MSA, the observed ratio will remain constant for a given concentration of HNO_3, all other things being equal. Although the ratio will remain constant, the overall sensitivity (concentration per ion ratio) is determined by the number of MSA monomer counts.

The resulting ions were electrostatically forced downstream toward the virtual iris/pinhole plates, while the subsequent neutral species were pumped away through annular ports located downstream of the ion-molecule reaction region at a flow of ~ 9 sLpm (~ 3 Lpm of sheath, ~6 Lpm of ambient air). The ions were directed by electric fields through a flow of 800 sccm nitrogen in front of a virtual iris consisting of two co-aligned 0.33 mm and 0.20 mm diameter orifices on 0.25 mm thick stainless steel plates separated by 0.76 mm. The flow of dry nitrogen in front of the pinhole helped to minimize ion clustering with water. The ~ 85 Torr pressure of the interstitial space between the virtual iris plates was kept constant to ensure that a constant stream of gas entered the vacuum system at all flight altitudes and pressures [*Mauldin et al., 1998a*].

Upon passing through the virtual iris, ions expanded supersonically into a differentially-pumped region of ~ 10^{-2} Torr where a series of additional lenses applied an electric field of ~ 2 V cm^{-1}. The field strength at these relatively low pressures resulted in collisions that broke apart a fraction of weakly bound clusters into their most acidic core ions [*Tanner and Eisele, 1995*]. Specifically, the electric field in this region was optimized to ensure that the signals from the desired clusters of interest, $MSA{\cdot}HNO_3$ at m/e 158 (for ambient) and $MSA{\cdot}H^{15}NO_3$ m/e 159 (for calibration), were maximized, and that weaker bound species (e.g. water clusters) were broken apart. The ions were focused by three lenses into a skimmer, by four more lenses into the quadrapole mass filters, and by one back lens into a Channeltron electron multiplier. With the exception of the virtual iris, all of the inlet remained outside the fuselage of the aircraft at ambient pressures.

The choice of ion chemistry for HNO_3 detection was particularly challenging for an airborne atmospheric pressure ionization scheme. *Mauldin et al.* [1998b] previously described a ground-based CIMS technique using bisulfate (HSO_4^-) as a reagent ion. Unfortunately,

difficulties in maintaining a constant source of reagent ion HSO_4^- were encountered. The gas phase concentration of sulfuric acid (H_2SO_4), the reagent ion precursor species, was difficult to control due to the intrinsically very low vapor pressure of sulfuric acid and its efficient ability to cluster with itself. Therefore, HSO_4^- reagent ion chemistry was an unreliable choice for use on an airborne platform where temperatures and relative humidities change rapidly. However, HSO_4^- reagent ion chemistry did show excellent sensitivity and selectivity for detection of HNO_3, and it was desired to keep these characteristics as much as possible. A compound of similar chemical structure and gas phase acidity was sought, but also one with significantly higher vapor pressures. To this end MSA, a derivative of sulfuric acid, was chosen. MSA is slightly more acidic (ΔG_{acid}= -1318 ± 8.4 kJ mol^{-1} for MSA; ΔG_{acid}= -1251 ± 13 kJ mol^{-1} for H_2SO_4) [*Koppel et al., 1994*] and its vapor pressure is several orders of magnitude higher than H_2SO_4 [*Ayers et al., 1980*; *Tang and Munkelwitz, 1991*]. Although MSA proved more reliable and easier to use than H_2SO_4, as will be described in detail later, controlling the concentration of MSA in the ion source under flight conditions remained problematic at times.

Results

Laboratory. A series of laboratory experiments were performed to examine the sensitivity of the ion chemistry to potential interferences expected in the atmosphere. Specifically, the nitrogen oxide species (NO_y) NO, NO_2, NO_3, and N_2O_5 were tested under dry and wet conditions (relative humidity with respect to water, RH_w, 0.001-100%) at NO_y mixing ratios far exceeding those expected in the troposphere. Experiments were conducted at two different mixing ratios of $H^{15}NO_3$ (80 pptv and 800 pptv) to examine if the MSA/HNO_3 and MSA/$H^{15}NO_3$ ion chemistry were perturbed by the addition of these species.

NO was prepared by filling a 5 L bulb with 10 Torr of a 0.5% NO/N_2 cylinder mixture and 960 Torr of N_2. A flow of 2 sccm from the bulb was passed through approximately one meter of 3.2 mm o.d., 1.6 mm i.d. nylon tubing to help remove any residual impurities of HNO_3 in the gas source (nylon is known to be an efficient scavenger of gas phase HNO_3). The flow was then diluted into 8000 sccm of zero air over the ion source resulting in a mixing ratio of 13 ppbv NO. No change in the ratio of the $H^{15}NO_3$/MSA (m/e 159) ratio was observed from the addition of the NO, nor was any increase observed for the HNO_3/MSA (m/e 158) ratio. These results indicate that NO neither produced HNO_3 in the ion source nor did it alter the HNO_3/MSA ion chemistry. Tests were done under both dry (0.001% RH) and wet (100% RH) conditions, and no noticeable change was observed in either case.

N_2O_5 was synthesized by the method of *Davidson et al.* [1978]. The N_2O_5 was stored in dry ice and kept in the dark when not in use. The N_2O_5 was differentially-pumped for several minutes prior to use at temperatures as high as 243 K. A flow of 93 sccm of N_2 was passed over the N_2O_5 which was kept in a dry ice/ethanol bath at 205 K. The vapor pressure of N_2O_5 at 205 K was approximately 6 mTorr [*McDaniel et al., 1988*]. It was assumed that the flow of nitrogen was saturated with the vapor pressure of N_2O_5 based upon *Cantrell et al.* [1988]. The N_2O_5-doped nitrogen flow passed through nylon tubing in order to ensure that any heterogeneous decomposition of N_2O_5 into HNO_3 would remain on the walls and not in the gas phase. The temperature of the gas handling line was kept at 298 K, and therefore, about 1% thermal decomposition of N_2O_5 into NO_3 and NO_2 occurred [*Cantrell et al., 1988*]. The residence time of N_2O_5 in the lines was approximately 30 s. The flow of N_2O_5-doped N_2 was diluted into 6000 sccm of zero air. Based on the vapor pressure and the flow rates, the concentration of N_2O_5 was 120 ppbv, while NO_2 and NO_3 were 1.2 ppbv. These experiments were also conducted under

wet and dry conditions, and no systematic differences were noted in either the ratio of the isotopically labeled $H^{15}NO_3 \cdot MSA$ or ambient $HNO_3 \cdot MSA$ signals.

Although NO, NO_2, NO_3, and N_2O_5 showed no observable interference in the $MSA \cdot HNO_3$ clusters under either wet or dry conditions, a significant change in sensitivity was observed with gas phase water. The vapor pressure of MSA is impacted by the relative humidity of water over the surface. Figure 3 shows the MSA ion counts for the monomer, dimer, trimer, and total counts of MSA versus relative humidity at 23ºC. At low relative humidities, a high percentage of MSA is tied up in the trimer (and likely higher clusters), with relatively little MSA in the monomer. As the humidity increases, the number of trimers decreases, while the number of dimers significantly increases. At RH=30%, the dimer population decreases, and at RH=65% the monomer becomes the dominant cluster. Overall, as the relative humidity increases, the vapor pressure of MSA decreases, and the cluster distribution moves toward the lower clusters. Therefore, one problem in using MSA reagent ion chemistry for HNO_3 detection is the changing sensitivity of the instrument as a function of ambient water vapor concentration. A more reliable way to introduce MSA and control its cluster distribution is needed, although the use of continual calibrations by the addition of $H^{15}NO_3$ helped to alleviate this problem.

Field studies. The NCAR CIMS HNO_3 instrument was flown on the NASA P3-B airplane as part of the NASA Transport and Chemical Evolution over the Pacific field experiment (TRACE-P) which took place February-April 2001 off the coast of eastern Asia (based in Hong Kong, PRC and Yokota Air Base, Japan). No data was collected during the transit flights 4-8 due to an ion source flooded with MSA vapor, which resulted in little or no ambient and calibration signals. Data from flight 9 was complicated by a lack of background and calibration signals resulting from large eddies removing both the isotopically-labeled calibration gas as well as the background zero air in the transport tube. The PFA cap shown in

Figure 2 was placed above transport tube before flight 10 to prevent the large eddies from disturbing calibration and background determinations. Therefore, data was archived from flights 10 onward, initially at 20 s resolution (flight 10 and 11) and at 5 s resolution thereafter. The measurement scheme generally involved a 20 s cycle as follows: 2 s for the MSA monomer at m/e 95, 1 s for MSA dimer at m/e 191, 3 s for the ambient signal (m/e 158), 3 s for calibration (m/e 159), 3 s for ambient, 1 s for an electronic noise background at m/e 20 (polarity of the Channeltron electron multiplier was reversed temporarily), 3 s for the ambient signal, 2 s for a partial mass scan at 0.5 s per amu from 20-160 amu, and another 3 s for an ambient measurement. In this way, HNO_3 was measured on average once every 5 s. The calibration signal at m/e 159 was only measured once every 20 s because its concentration was well controlled. Likewise, the concentration of reagent ion was fairly constant on a 20 s timescale as well. On occasion, the time of the partial mass scan was shortened or eliminated during portions of flights to measure other masses of interest.

The duct and transport tube were not actively heated in-flight, and therefore sampled air was only warmed by adiabatic compression from the slowing of the air inside the inlet and from conduction of heat from inside to outside of the instrument. In combination, temperature readings around the transport tube suggest a warming of at most 5-10 K above ambient temperatures. Occasionally, under very cold conditions (T < -15ºC), it was necessary to heat the ion source region to raise the vapor pressure of MSA to ensure adequate amounts of reagent ion signal (> 500 cts s^{-1}). Under no conditions did the ion source temperature exceed 23ºC while in-flight. Due to the very short transit time in the ion source (50 ms), it appears unlikely that the ambient air warmed sufficiently for desorption of particulate nitrates.

For warm (T>10ºC) and very dry (T_d<0ºC) conditions, sufficiently high vapor pressures of MSA would result in clustering of MSA into the dimer, which does not readily cluster with

HNO_3. Therefore, it was necessary to humidify the sheath flow to increase the monomer MSA ion. A fraction (0-1.4 sLpm) of ~ 3 sLpm sheath flow was bubbled through a 300 ml ~ 0.01 M aqueous sodium hydroxide (NaOH) solution to tie up any residual NO_3^- in the water (Aldrich, HPLC grade). The humidified flow was passed into an empty vessel to ensure that any small droplets would settle or collide with the container walls before entering the ion source. Finally, the sheath flow passed through a 0.9 micron nylon filter as well as a sodium bicarbonate ($NaHCO_3$) filter to remove any small (micron-sized) particles. The use of a humidified sheath flow was incrementally adjusted to keep the signal of the MSA dimer to approximately one-third of the monomer. At colder temperatures (<10ºC ambient), a low dimmer signal (due to lower vapor pressure of MSA) precluded the need for a humidified sheath flow.

Because the signal of the monomer ion of MSA changed with ambient conditions, the sensitivity of the HNO_3 signal (ion ratio m/e 158:m/e 95) changed depending upon ambient conditions. In the laboratory, sensitivities of the MSA-HNO_3 cluster were routinely 1-3 counts $pptv^{-1}$ s^{-1}. In contrast, in-flight operation of the instrument decreased the sensitivity by an order of magnitude relative to the laboratory experiments due to decreased gas flow into the vacuum system in order to accommodate the the other two channels - OH/MSA/H_2SO_4, HO_2/RO_2 and due to non-optimal pressures in the collision chamber (again, a compromise of the multi-channel shared vacuum housing). Although in-flight sensitivities of the cluster at times approached 1 ct $pptv^{-1}$ s^{-1}, more typical values were 0.1-0.4 cts $pptv^{-1}$ s^{-1} during TRACE-P. Therefore, it was necessary to continuously calibrate with a flow of isotopically-labeled $H^{15}NO_3$ at the top of the transport tube at all times.

Background estimates of HNO_3 sticking to instrument surfaces could be experimentally-determined by three different methods. The first method involved adding a large flow of zero air to the very top of the transport tube, just upstream from the addition of the calibration gas (not

shown in Figure 2 for clarity). Although this method worked reasonably on the ground, in-flight tests showed little effect even at zero air flows several sLpm greater than the flow down the transport tube. Because the transport tube lies perpendicular to the main flow in the large inlet, significant eddies formed in the upper region of the transport tube, and it is thought that large (though unquantified) amounts of the zero air were turbulently ejected from the inlet. Thus, this method was not used to estimate backgrounds while in-flight.

A second method involved overfilling the inlet with a flow of zero air just above the ion source. This method effectively examined the adsorption of HNO_3 to the metal pieces of the ion source, although it could not be used to estimate the amount of HNO_3 adsorbed to the extruded PFA upper transport tube. Figure 4 shows the responses of the ambient and calibration signals as zero air was added in front of the ion source during an 18 minute segment of Flight 16 (Yokota local #2) at an altitude of 17,500' (674 mb) while crossing the island of Japan. The signals have been normalized to their initial respective values when no zero air was being added. The zero point on the abscissa is the equivalence point where the amount of gas being drawn down the ion source is balanced by the flow of zero air above the ion source. Data below this point are considered "underfilling" the transport tube, while data above this is considered "overfilling" the transport tube.

In theory, the calibration signal should remain unchanged until the equivalence point. That is, the concentration of the calibration gas is independent of whether it is diluted by ambient air or by zero air. However, beyond the equivalence point when the inlet is overfilled, the flow of zero air through the transport tube is away from the ion source, and therefore, the concentration (and hence signal) of the calibration gas should be at background levels. For the case of the ambient signal, however, a flow of zero air decreases the amount of ambient air pulled into the ion source. Therefore, the response of the ambient signal should linearly depend

on the overfill flow. The theoretical curves for each case are shown in Figure 4 in dotted lines for the calibration and ambient signals.

In-situ field tests indicated that the responses of the signals differed from the expected behavior. Specifically, for the calibration gas, a sigmoid curve is observed – initially flat, showing no response as zero air is added and then rapidly decreasing when approaching within 2 sLpm of the equivalence point. No significant decrease in the signal was observed from slightly beyond the equivalence point to over 2 sLpm overfill. The calibration data suggests that turbulent eddies partially removed $H^{15}NO_3$ from the upper part of the transport when nearing the equivalence point. The data also show that overfilling the transport tube by greater than 2 sLpm of the equivalence flow was sufficient to record background conditions of calibration gas.

In contrast to the isotopically labeled $H^{15}NO_3$, the response of the ambient signal more closely resembles the expected behavior. The measured signals were only slightly higher than the theoretical behavior. Not all of the zero air was drawn into the ion source when underfilling, but some small fraction was "pulled out" of the upper transport tube. Nonetheless, the amounts were quite small, and the general behavior was linear to first order. In addition, the ambient background was constant from the equivalence point to beyond 2 sLpm overfilling. Therefore, all backgrounds measured by flowing zero air above the ion source were done at overfills at least 2 sLpm beyond the equivalence point. Finally, the ambient concentration of HNO_3 may have changed during the in-flight test, and therefore, the results are potentially complicated by this factor. However, other chemical species such as NO_y, NO, O_3, and CO indicated a relatively homogeneous airmass during the time of this test.

Similar tests like the one described above were conducted throughout TRACE-P. Data was entirely consistent with the results shown here, whether at low altitude (500' above sea level) or at high altitude (17,000'). A slight dependence was observed based on airspeed with

higher speeds having greater turbulence in the transport tube. For example, the sigmoid fit to the calibration curve in Figure 4 has a half-mean decay constant at –0.97 ± 0.05 sLpm with respect to equivalence at an airspeed of 297 knots. In contrast, speeds of 330 knots had –1.68 ± 0.03 sLpm while slower speeds of 274 knots had –0.94 ± 0.05 sLpm. Although pressure may indeed affect the degree of turbulence in the upper transport tube, the effect appeared to be caused by airspeed. A comparison of similar pressures (554, 516 mb) with different airspeeds (321, 308 knots, respectively) indicated slightly more turbulence (decay constants of -1.24 ± 0.13 vs 1.05 ± 0.15) with the higher airspeeds.

Figure 5a shows a representative background when overfilling the inlet with zero-air on Flight 14 (Okinawa to Yokota transit) at an altitude of 500'. The concentration of the calibration gas was 540 pptv while the average HNO_3 mixing ratio was ~ 470 pptv. Upon overfilling the inlet, both the ambient and calibration signals decreased to the same respective levels of < 0.005 ion ratio. In addition, the ambient HNO_3 data, with a temporal resolution of once every 5 seconds, shows that the background signal was achieved within the 5 s measurement time, and no significant decrease was observed for the duration of the overfill. Likewise, the signal responded within the 5 s measurement resolution when the overfilling was stopped. These results indicate that the background was a very small percentage of the overall signal, and that HNO_3 adsorbed to the metal surfaces of the ion source did not significantly affect the measurement.

Figure 5b shows a background of HNO_3 at much lower concentrations of ~ 80 pptv taken at 17,300' (509 mb, -9ºC) on Flight 23 (Kona to Dryden transit). Like the previous example, the background ion ratios were ~ 0.005. Despite the much closer difference in signal to background ion signal ratios and the relatively low concentration of HNO_3, the response of the instrument to the background measurement remained rapid, on the timescale of the temporal resolution (5 s).

In addition, the overall background of the measurements indicated a limit of detection of ~ 5 pptv.

Finally, a third way to measure the background involved the removal of the calibration flow at the top of the upper transport tube. This method estimated the amount of HNO_3 adsorbed to the extruded PFA transport tube. Simply turning off the flow of the calibration gas was insufficient to test for a background as any small flows into the transport tube would still emit $H^{15}NO_3$. Therefore, it was necessary to reverse the flow of the calibration gas by pumping on the calibration tube about one meter downstream of the end of the calibration tube. Figure 6 shows a representative example of the response of 515 pptv of the calibration signal upon pumping on the flow on Flight 14 at 14,300' (577 mb, -5ºC). In the 20 s time resolution of the calibration measurement, the signal decreased to a value indistinguishable from the background level. The extruded PFA transport tube showed minimal wall/surface effects from the removal of calibration $H^{15}NO_3$. However, because the inside surfaces of the long, thin tubing that carried the isotopically labeled $H^{15}NO_3$ flow had to re-equilibrate to a new concentration, relatively long periods of time (2-20 min) were needed to ensure the isotopic signal was stable again. Additionally, pumping on the calibration gas line pulled some amount of ambient HNO_3 into the calibration line. Thus, this background measurement was conducted only about once per flight, mainly to ensure that the extruded PFA transport tube remained a minimal sink for gas phase HNO_3.

Although the background signal at masses 158 and 159 remained small throughout the field campaign, several factors contributed to its presence. Electronic noise (< 1 ct s^{-1}) in the channeltron electron multiplier was determined by the signal at m/e 20 when the polarity of the quadrupole lenses was reversed. Desorption of HNO_3 off instrument surfaces and walls and any production of HNO_3 from the high energy ionization near the americium-241 were measured

through the tests noted above. The largest sources of background signals at masses 158 and 159 originated from isotopic contributions of significant peaks near m/e 156 and m/e 157. The m/e 156 and 157 peaks correlated with the availability of MSA reagent ions and thus were assumed to contain MSA. The remaining part of the cluster most likely resided at m/e 60 and m/e 61, CO_3^- and HCO_3^-, and indeed these species were abundant in mass spectra taken throughout the experiment. At concentrations of HNO_3 < 100 pptv, these peak signals were often larger (factor of 2-5) than the ambient signal. Although the resolution of the mass spectrometer was such that only around 1% of adjacent ions were measured (m/Δm=320), the isotopic abundances of the likely elements - sulfur (^{33}S=0.76%, ^{34}S=4.22%), carbon (^{13}C=1.11%), oxygen (^{17}O=0.037%, ^{18}O=0.204%), and nitrogen (^{15}N=0.37%) - resulted in significant mass counts at the ambient and calibration signals (m/e = 158, 159). The signals at m/e 156 and m/e 157 were measured every 20 s during portions of several flights and no obvious dependence on sheath flow, pinhole flow, or zero air was observed. In addition, on all flights these species were measured at least once every 10 minutes during partial but continual mass scans as part of the measurement scheme. No apparent correlation was observed with any factor besides increasing or decreasing with MSA monomer abundance. It remains unclear how or why these species would cluster so readily with MSA or be so abundant in the ion source, but they most likely form before MSA ions are introduced.

Additional background contributions at the ambient signal derived from signals from adjacent masses (1%) and the impurity of the $H^{15}NO_3$ calibration source (0.6%). In total, the m/e 158 signal had contributions from the following sources:

$$\text{measured m/e 158 signal} = 5.4\%(v) + 4.24\%(w) + x + 1.4\%(y) + 0\%(z)$$

where v, w, x, y, and z correspond to the "real" signals (effects of isotopes removed, adjacent masses removed, etc.) at masses 156, 157, 158,159, and 160 signals, respectively. A linear set of

equations for each of the five masses was solved taking into account all of these factors on one another. Generally, the size of this correction was small (< 10%) for the ambient signal at mixing ratios > 100 pptv HNO_3 but became increasingly significant at lower mixing ratios. Ultimately, the correction for the relatively large peaks at m/e 156 and m/e 157 accounted for most of the background in the lower concentration data and was the single largest source of error in the measurements at low (< 100 pptv) concentrations. Overall error (± 2σ) of the measurement including systematic and random errors were the limit of detection (5 pptv) plus the following: ± 25% pptv at mixing ratios < 100 pptv, ± 20% from 100-200 pptv, and ± 15% for mixing ratios > 200 pptv.

Calibrations of the system occurred by the addition of the isotopically labeled $H^{15}NO_3$ in the transport tube. The $H^{15}NO_3$ source contained 99.6% enrichment of 15N-nitric acid and was enclosed in a permeation tube (Vici). The tube was initially reported with an emission rate of 57 ng min^{-1}, however permeation tubes are notorious for different emission rates under different conditions [*Talbot et al., 1997; Ryerson et al., 1999*]. Therefore, the permeation tube was held in a heated cavity with a critical orifice of 7 cm of 0.06 mm i.d. PFA tubing. The permeation tube was always kept at a constant pressure of 35 psi N_2 during the mission (except when changing tanks). An inert flow meter (Teflon internal surfaces) upstream of the permeation tube measured the flow (~ 100 sccm), and the pressure over the tube was regulated to 35 psi. In this way, N_2 was continually flowing over the permeation source at a constant pressure even when the aircraft had no power. Finally, the flow over the permeation cell passed through a manifold where a portion (0-100 sccm) of the flow could be removed by pumping, while the remaining amount joined a carrier flow of ~ 100 sccm N_2. The carrier/calibration flow passed through ~ 40 cm of 1.1 mm o.d., 0.6 mm i.d. PFA tubing. The carrier/calibration tubing was enclosed by 1.3 mm i.d.

stainless steel tubing which was resistively heated to 45ºC from just inside the fuselage to the outside edge of the transport tube.

Temperature control of the permeation tube consisted of an aluminum thermofoil backed, resistive heater (Minco) and a temperature controller (Watlow, model 241). The permeation tube was kept at a constant temperature of 40ºC except when the airplane was powered down. Before flight, the temperature of the permeation cell was raised to 40ºC at least 2 hours before measurements commenced. Ground-based tests indicated that one hour was sufficient for the tubing walls to re-equilibrate to a new permeation rate and subsequent changes in $H^{15}NO_3$ concentration. The mass of the permeation cell was measured for eight months after the end of the deployment, and a constant emission rate of 33.5 ± 1.3 ng min^{-1} was obtained as shown in Figure 7. Although no mass measurements were made in the field, the output of the permeation cell was measured twice in the field by the University of New Hampshire mist chamber/ion chromatography instrument on the NASA DC-8 airplane. The UNH measurements yielded an average of 29 ± 1 ng min^{-1} for three measurements before P-3B flight 17, and 32 ± 2 ng min^{-1} for two measurements before P-3B flight 23. The mass data and the two ion chromatography measurements agreed to within 15%, and it provides strong evidence that the permeation cell emitted $H^{15}NO_3$ at a rate near 33.5 ng min^{-1} during the entire TRACE-P campaign. The overall accuracy of the permeation cell calibration was the largest source of error for measurements above 200 pptv.

Multipoint calibrations were conducted in-flight to examine the linearity and response of the measured $H^{15}NO_3$ signal versus $H^{15}NO_3$ concentration. Typically, multipoint calibrations were conducted at least once per flight for flights 16-24. To conduct these experiments, a known amount of the calibration gas was removed before flowing into the inlet. A representative example of an in-flight calibration is shown in Figure 8 for a wide range of altitudes and mixing

ratios (50-2500 pptv) during Flight 16 (Yokota local #2). Despite the much different environments of the data (ranging from 17,000 feet to the marine boundary layer), a linear response is clearly noted in the data in Figure 8, suggesting that the continuous single-point calibrations throughout the rest of the flight were valid. Although the absolute calibration factor and sensitivity did change from flight to flight and within a flight (mainly due to the impact of MSA clustering on the availability of MSA monomer as noted previously), the overall sensitivity was generally around 2000-3000 pptv/ion ratio.

Intercomparisons. Three brief and informal intercomparisons between instruments onboard the NASA P-3B and NASA DC-8 were conducted during TRACE-P. Typical distances between the airplanes ranged from 0.2-1.0 km with a vertical separation of less than 100 m. For more information on the intercomparisons, refer to *Eisele et al.* (this issue). During the first intercomparison on the transit to Hong Kong, no data were obtained due to a lack of reagent ion signal and calibration signal (MSA had coated the ion source and reagent monomer MSA signals were extremely small). NCAR CIMS recorded no data on the second (P3 flight #16, DC flight #10) and third (P3-flight #23, DC flight #20) intercomparisons, and the results were compared to the HNO_3 measurements from the mist chamber/ion chromatograph instrument from the University of New Hampshire onboard the DC-8 aircraft (UNH). Details of the UNH instrument are described elsewhere (*Talbot et al., 1997, 1999, this issue*). It should be noted that each instrument detected HNO_3 with a different technique (chemical ionization versus ion chromatography), vastly different inlets, and independent permeation standards (though as noted above, within 15% of one another).

Figure 9a shows the data collected on the second intercomparison, lasting about 24 minutes at 17,000'. No data was collected in the final 3 minutes of the intercomparison from NCAR CIMS due to turbulence issues arising from an overfill flow near the equivalence point.

The light blue solid line shows the NCAR CIMS HNO_3 data collected every 5 seconds. The red line shows the UNH measurements. Finally, the dark blue line shows the NCAR CIMS measurements averaged within the UNH sampling window. Reasonable agreement is observed between measurements with NCAR CIMS reporting an average of 158 ± 32 pptv (N=224, 1σ) in 5 s measurements compared to 185 ± 28 pptv (N=9) for the UNH samples of 120-180 s. The averages were within the error bars of ± 20% for NCAR and ± 15% for UNH. On a point by point basis, CIMS was lower than UNH on 6 of 9 points, with a mean deviation of UNH greater than NCAR by 23 pptv and a standard deviation of the mean of 29 pptv. It is unclear why three data points lie outside of each other's error bars or why NCAR had lower measurements than UNH, and potential sources of disagreements are noted later.

Figure 9b shows the results of the third intercomparison over the Pacific Ocean just east of Hawaii. This intercomparison consisted of 20 minutes at 17,000', followed by a descent at 500' per minute to 500', and 20 minutes at 500'. A problem with electrical noise in the OH channel of the four channel system prevented data collection for a 7 minute period on the descent for NCAR CIMS. Both techniques measured low values of HNO_3 during the high-altitude portion. CIMS measured on average 12 pptv higher than UNH during the high-altitude portion, with the exception of a spike measured only by UNH around 18:24 UT. On the descent, both techniques measured a local maximum of 190 pptv HNO_3 around 10,000 feet and subsequent decrease to < 100 pptv near the end of the descent. A gradual rise of HNO_3 was measured by both instruments during the boundary layer run. A significant deviation between the datasets did appear near the end of the boundary layer run with CIMS HNO_3 measuring 72 pptv higher than the values obtained by UNH. No other tracers identified significant deviations, and therefore, a change in airmass is not likely a valid reason for the discrepancy. Overall, the mean deviation

between the measurements indicates that CIMS was 15 pptv higher than UNH throughout the intercomparison.

One potential reason for the discrepancies between the two measurements is the sampling of nitrate-containing particles (< 2.5 μm aerodynamic diameter) by UNH's instrument. The NCAR CIMS inlet was not expected to directly sample particles because only gas phase ions (not charged particles) were electrostatically directed into the vacuum system. Sampling of nitrate-containing particles would result in higher measurements of gas phase HNO_3 relative to the true amount. Particulate nitrate smaller than 1.3 μm diameter was measured onboard the P-3B [*Ma et al., this issue; Weber et al., 2001*]. The second intercomparison showed steadily increasing levels of particulate nitrate from 22 to 44 pptv, and UNH measurements indeed averaged 27 pptv higher than NCAR CIMS. Particulate nitrate on the third intercomparison were generally below 20 pptv, and yet NCAR CIMS reported higher measurements than UNH. Therefore, the differences between the HNO_3 measurements could not be explained by the amount of particulate nitrate measured onboard the P-3B. A more thorough analysis on the size distributions of nitrate-containing aerosol particles is ultimately needed to quantify how the sampling of particulate nitrate may impact HNO_3 measurements.

Figure 10 shows a plot of the NCAR measurements versus UNH measurements for all of the datapoints in the second and third intercomparisons. The associated error bars for the measurements are determined using the stated errors mentioned previously for NCAR CIMS and the uncertainties of UNH stated in the TRACE-P data archive: ±30% for < 20 pptv, ±25% for 20-25 pptv, ±20% for 25-100 pptv, and ±15% for > 100 pptv. The uncertainties of each measurement technique for the data in Fig. 10 differ from the more general ones used by *Eisele et al.* [this issue]. The error limits shown in Figure 10 are the square root of the sum of the errors squared for each measurement. The slope of the data is 0.94 ± 0.18 (2σ), showing general

agreement between techniques, although an offset of 19 ± 14 pptv (2σ) indicates that potential disagreements may be related to background issues. Overall, 29 out of the 40 datapoints lie within the expected error bars of each set of measurements, and 8 of the 11 discrepancies lie at mixing ratios below 100 pptv. Clearly, the two techniques appear to be in good agreement, although issues such as background determinations and aerosol particle sampling most likely need to be better quantified, especially at low mixing ratios.

Finally, the response of the inlet and instrument to rapid changes in ambient HNO_3 concentration is demonstrated. Figure 11a shows the response of the instrument to ship plumes at 500' above the South China Sea on Flight 14 (Okinawa to Yokota transit). A uniform atmospheric concentration of ~ 450 pptv prevailed, although individual spikes as high as 1800 pptv occurred during the 5 s measurement resolution time for this flight. In addition, multiple decreases and increases occurred, showing that the ability of the inlet to resolve rapid HNO_3 changes and also return to baseline values. If significant amounts of HNO_3 had been adsorbed onto the inlet (e.g. if the "true" value of the peaks were 5 ppbv), one would expect to observe desorption of HNO_3 off the inlet surfaces with corresponding increases in the atmospheric background level of ~ 450 pptv during this time. For comparison, the corresponding changes for NO_y (1 s resolution) as measured by the University of Tokyo are also shown (*Kondo et al., 1997; Koike et al., 2000; Miyazaki et al., this issue*). Tight correlation is observed, indicating very good resolution of the inlet. No attempts have been made to resolve the ~ 3 s offset between the measurements. Figure 11b shows a vertical profile of HNO_3 during descent into the marine boundary layer where highly polluted air was encountered. Upon entering the polluted layer, ambient HNO_3 increases from around 360 pptv to 1600 pptv in 15 s. The rapid changes presented in Figure 11, in combination with in-flight tests of the calibration gas, suggest that

HNO_3 adsorption onto inlet surfaces was not a significant problem and therefore generally did not interfere with the measurement.

Summary and future work. Nitric acid was detected using a unique choice of inlet design and materials and selective ion chemical ionization mass spectrometry using methanesulfonic acid as a reagent ion. The instrument measured HNO_3 every 5 s with a limit of detection of 5 pptv. The inlet was not actively heated to prevent possible desorption of particulate nitrates into gas phase HNO_3. The instrument was calibrated continuously using isotipcally labeled $H^{15}NO_3$, and the inlet demonstrated very few problems of surface adsorption. Intercomparisons with a more established HNO_3 measurement technique by UNH were promising.

Future areas of improvement with this instrument include identifying a more reliable way to introduce methanesulfonic acid or selecting a more stable reagent ion. Under low concentrations of reagent ion, the sensitivity of the measurement decreased significantly. One possibility to better control MSA reagent concentration includes using a reduced pressure ion source with extruded PFA surfaces. Although MSA worked favorably for this campaign, future research will examine ways to control the addition of MSA to the ion source (as opposed to manually placing MSA droplets in the ion source). Furthermore, the presence of unknown peaks at m/e 156 and m/e 157 can significantly deplete the availability of reagent ion MSA, and solving this problem will enhance the sensitivity of the technique. Nonetheless, the techniques described here are a start toward quantifying and ultimately better understanding the chemistry of HNO_3 in the troposphere.

Acknowledgements. MAZ gratefully acknowledges support from an NCAR ASP Postdoctoral Fellowship. The authors thank J. Dibb, E. Scheuer, and R. Talbot for invaluable assistance and

advice in the calibration of the permeation standard and for great cooperation in the intercomparisons. We also thank J. Orlando and G. Tyndall for the use of their N_2O_5, J. Fox and the ATD instrument shop for inlet design and construction, J. Vanderpol for shop work, T. Ryerson of the NOAA AL for permeation cell oven plans, and R. Hendershot and W. Bradley for electronics assistance. Finally, all of this work would not have happened without the helpful assistance of the NASA TRACE-P Science Team and aircraft support personnel at NASA Wallops Flight Facility. The National Center for Atmospheric Research is operated by the University Corporation for Atmospheric Research under sponsorship of the National Science Foundation.

References

Abbatt, J.P.D., "Interaction of HNO_3 with water-ice surfaces at temperatures of the free troposphere", *Geophys. Res. Lett., 24*, 1479-1482, 1997.

Adams, P.J., J.H. Seinfeld, and D.M. Koch, "Global concentrations of tropospheric sulfate, nitrate, and ammonium aerosol simulated in a general circulation model", *J. Geophys. Res*., *104*, 13791-13823, 1999.

Arnold, F., J. Scheid, T. Stilp, H. Schlager, and M.E. Reinhardt, "Measurements of jet aircraft emissions at cruise altitude I: the odd-nitrogen gases NO, NO_2, HNO_2, and HNO_3", *Geophys. Res. Lett., 12*, 2421-2424, 1992.

Ayers, G.P., R.W. Gillett, and J.L. Gras, "On the vapor pressure of sulfuric acid", *Geophys. Res. Lett., 7*, 433-436, 1980.

Christopher A. Cantrell, G. D. Edwards, S. Stephens, R. L. Mauldin, M. Zondlo, E. Kosciuch, F. L. Eisele, R. E. Shetter, B. L. Lefer, S. Hall, F. Flocke, A. Weinheimer, A. Fried, E. Apel, Y. Kondo, D. R. Blake, N. Blake, I. Simpson, A. Bandy, D. Thornton, B. Heikes, H. Singh, W. Brune, H. Harder, M. Martinez-Harder, M. A. Avery, S. Vay, J. D. Barrick, G. W. Sachse, J. R. Olsen, J. H. Crawford, "Peroxy Radical Behavior during TRACE-P as Measured Aboard the NASA P-3B Aircraft", submitted to the TRACE-P special issue, *J. Geophys. Res.*, 2002.

Cantrell, C.A., J.A. Davidson, A.H. McDaniel, R.E. Shetter, and J.G. Calvert, "The equilibrium constant for $N_2O_5 \Leftrightarrow NO_2 + NO_3$: absolute determination by direct measurement from 243-273 K", *J. Chem. Phys., 88*, 4997-5006, 1988.

Davidson, J.A., A.A. Viggiano, C.J. Howard, I. Dotan, F.C. Fehsenfeld, D.L. Albritton, and E.E. Ferguson, "Rate constants for the reactions of O_2^+, NO_2^+, NO^+, H_3O^+, CO_3^-, NO_2^-, and halide ions with N_2O_5 at 300 K", *J. Chem. Phys., 68*, 2085-2087, 1978.

Dentener, F.J., G.R. Carmichael, Y. Zhang, J. Lelieveld, and P.J. Crutzen, "Role of mineral aerosol as a reactive surface in the global troposphere", *J. Geophys. Res.*, *101*, 22869-22889, 1996.

Eisele, F.L., R.L. Mauldin, D.J. Tanner, J.R. Fox, T. Mouch, and T. Scully, An inlet/sampling duct for airborne OH and sulfuric acid measurements, *J. Geophys. Res., 102*, 27993-28001, 1997.

Eisele, F.L., L. Mauldin, C. Cantrell, M. Zondlo, E. Apel, A. Fried, J. Walega, R. Shetter, B. Lefer, F. Flocke, A. Weinheimer, M. Avery, S. Vay, G. Sachse, H.B. Singh, W. Brune, H. Harder, M. Martinez, A. Bandy, D. Thornton, B. Heikes, Y. Kondo, D. Riemer, S. Sandholm, D. Tan, R. Talbot, and J. Dibb, "Summary of measurement intercomparisons during TRACE-P", submitted to the TRACE-P Special Issue, *J. Geophys. Res*.

Jacob, D.J., B. Heikes, S.-M. Fan, J.A. Logan, D.L. Mauzerall, J.D. Bradshaw, H.B. Singh, G.L. Gregory, R.W. Talbot, D.R. Blake, G.W. Sachse, "Origin of ozone and NO_x in the tropical troposphere: a photochemical analysis of aircraft observations over the South Atlantic basin", *J. Geophys. Res., 101*, 24235-24250, 1996.

Kerminen, V.-M., A.S. Wexler, and S. Potukuchi, "Growth of freshly nucleated particles in the troposphere: roles of NH_3, H_2SO_4, HNO_3, and HCl", *J. Geophys. Res., 102*, 3715-3724, 1997.

Kondo, Y., S. Kawakami, M. Koike, D.W. Fahey, H. Nakajima, Y. Zhao , N. Toriyama, M. Kanada, G.W. Sachse, and G.L. Gregory, The performance of an aircraft instrument for the measurement of NO_y, *J. Geophys. Res., 102*, 28663-28671, 1997.

Koike, M., Y. Kondo, G.L. Gregory, B.E. Anderson, G.W. Sachse, D. Blake, H.B. Singh, A. Thompson, K. Kita, Y. Zhao, T. Sugita, R. Shetter, H. Ikeda, S.C. Liu, L. Jeagle, and N. Toriyama, Impact of aircraft emissions on reactive nitrogen over the North Atalantic Flight Corridor region, *J. Geophys. Res., 105*, 3665-3677, 2000.

Koppel, I.A., R.W. Taft, F.A. Anvia, S.-Z. Zhu, L.-Q. Hu, K.-S. Sung, D.D. DesMarteau, L.M. Yagupolskii, Y.L. Yagupolskii, N.V. Ignat'ev, N.V. Kondratenko, A.Y. Volkonskii, V.M. Vlasov, R. Notario, and P.-C. Mari, "The gas-phase acidities of very strong neutral bronsted acids", *J. Am. Chem. Soc., 116*, 3047-3057, 1994.

Laaksonen, A., J. Hienola, and M. Kulmala, "Supercooled cirrus cloud formation modified by nitric acid pollution of the upper troposphere", *Geophys. Res. Lett., 24*, 3009-3012, 1997.

Liang, J., L.W. Horowitz, D.J. Jacob, Y. Wang, A.M. Fiore, J.A. Logan, G.M. Gardner, and J.W. Munger, "Seasonal budgets of reactive nitrogen species and ozone over the United States, and export fluxes to the global atmosphere", *J. Geophys. Res.*, *103*, 13435-13450, 1998.

Lin, J.-S., and A. Tabazadeh, "The effect of nitric acid uptake on the deliquescence and efflorescence of binary ammoniated salts in the upper troposphere", *Geophys. Res. Lett.*, 10.1029/2002GL015251, 2002.

Ma, Y., R.J. Weber, Y.-N. Lee, D.C. Thornton, A.R. Bandy, A.D. Clarke, D.R. Blake, G.W. Sachse, H.E. Fuelberg, C.M. Kiley, J.-H. Woo, D.G. Streets, G.R. Carmichael, F.L. Eisele, "The Characteristics and Influence of Biomass Burning Aerosols on Fine Particle Ionic Composition Measured in Asian Outflow During TRACE-P", submitted to the TRACE-P special issue, *J. Geophys. Res.*

Mauldin, R.L., D.J. Tanner, and F.L. Eisele, "Measurements of OH during PEM-Tropics A", *J. Geophys. Res., 104*, 5817-5827, 1999.

Mauldin, R.L., G.J. Frost, G. Chen, D.J. Tanner, A.S.H. Prevot, D.D. Davis, and F.L. Eisele, "OH measurements during the First Aerosol Characterization Experiment (ACE 1): observations and model comparisons", *J. Geophys. Res., 103*, 16713-16729, 1998a.

Mauldin, R.L., D.J. Tanner, and F.L. Eisele, "A new chemical ionization mass spectrometer technique for the fast measurement of gas phase nitric acid in the atmosphere", *J. Geophys. Res*., *103*, 3361-3367, 1998b.

McDaniel, A.H., J.A. Davidson, C.A. Cantrell, R.E. Shetter, and J.G. Calvert, "Enthalpies of formation of dinitrogen pentoxide and the nitrate free radical", *J. Phys. Chem., 92*, 4172-4175, 1988.

Meng, Z., D. Dabdub, and J.H. Seinfeld, "Chemical coupling between atmospheric ozone and particulate matter", *Science, 277*, 116-119, 1997.

Miller, T.M., J.O. Ballenthin, R.F. Meads, D.E. Hunton, W.F. Thorn, and A.A. Viggiano, "Chemical ionization mass spectrometer technique for the measurement of HNO_3 in air traffic corridors in the upper troposphere during the SONEX campaign", *J. Geophys. Res., 105*, 3701-3707, 2000.

Möhler, O. and F. Arnold, "Flow reactor and triple quadrupole mass spectrometer investigations involving nitric acid: implications for atmospheric HNO_3 detection by chemical ionization mass spectrometry", *J. Atmos. Chem., 13*, 33-61, 1991.

Miyazaki, Y., , Y. Kondo, M. Koike, K. Kita, N. Takegawa, H. E. Fuelberg, G. W. Sachse, F. Flocke, A. J. Weinheimer, H. B. Singh, M. Zondlo, R. W. Talbot, S. T. Sandholm, M. A. Avery, and D. R. Blake, "Synoptic-scale transport of reactive nitrogen over the western Pacific in spring", submitted to the TRACE-P Special Issue, *J. Geophys. Res*.

Neuman, J.A., L.G. Huey, R.W. Dissly, F.C. Fehsenfeld, F. Flocke, J.C. Holecek, J.S. Holloway, G. Hubler, R. Jakoubek, D.K. Nicks Jr., D.D. Parrish, T.B. Ryerson, D.T. Sueper, and A.J. Weinheimer, "Fast-response airborne in situ measurements of HNO_3 during the Texas 2000 Air Quality Study", *J. Geophys. Res., doi:10.1029/2001JD001437*, 2002.

Neuman, J.A., R.S. Gao, M.E. Schein, S.J. Ciciora, J.C. Holecek, T.L. Thompson, R.H. Winkler, R.J. McLaughlin, M.J. Northway, E.C. Richard, and D.W. Fahey, "A fast-response chemical ionization mass spectrometer for in situ measurements of HNO_3 in the upper troposphere and lower stratosphere", *Rev. Sci. Instrum.*, *71*, 3886-3894, 2000.

Neuman, J.A., L.G. Huey, T.B. Ryerson, and D.W. Fahey, "Study of inlet materials for sampling atmospheric nitric acid", *Envi. Sci. Tech.*, *33*, 1133-1136, 1999.

Reiner, T., O. Mohler, and F. Arnold, "Improved atmospheric trace gas measurements with an aircraft-based tandem mass spectrometer: Ion identification by mass-selected fragmentation studies", *J. Geophys. Res., 103*, 31309-31320, 1998.

Ryerson, T.B., L.G. Huey, K. Knapp, J.A. Neuman, D.D. Parrish, D.T. Sueper, and F.C. Fehsenfeld, "Design and initial characterization of an inlet for gas-phase NO_y measurements from aircraft", *J. Geophys. Res., 104*, 5483-5492, 1999.

Schneider, J., F. Arnold, V. Burger, B. Droste-Franke, F. Grimm, G. Kirchner, M. Klemm, T. Stilp, K.-H. Wohlfrom, "Nitric acid (HNO_3) in the upper troposphere and lower stratosphere at midlatitudes: new results from aircraft-based mass spectrometric measurements", *J. Geophys. Res., 103*, 25337-25343, 1998.

Singh, H.B., D. Herlth, R. Kolyer, L. Salas, J.D. Bradshaw, S.T. Sandholm, D.D. Davis, J. Crawford, Y. Kondo, M. Koike, R. Talbot, G.L. Gregory, G.W. Sachse, E. Browell, D.R. Blake, F.S. Rowland, R. Newell, J. Merrill, B. Heikes, S.C. Liu, P.J. Crutzen, M. Kanakidou, "Reactive nitrogen and ozone over the western Pacific: distribution, partitioning, and sources", *J. Geophys. Res., 101*, 1793-1808, 1996.

Singh, H.B., W. Viezee, Y. Chen, A.N. Thakur, Y. Kondo, R.W. Talbot, G.L. Gregory, G.W. Sachse, D.R. Blake, J.D. Bradshaw, Y. Wang, and D.J. Jacob, "Latitudinal distribution of reactive nitrogen in the free troposphere over the Pacific Ocean in late winter/early spring", *J. Geophys. Res., 103*, 28237-28246, 1998.

Talbot, R.W., J.E. Dibb, B.L. Lefer, E.M. Scheuer, J.D. Bradshaw, S.T. Sandholm, S. Smyth, D.R. Blake, N.J. Blake, G.W. Sachse, J.E. Collins, and G.L. Gregory, "Large-scale distributions of tropospheric nitric, formic, and acetic acids over the western Pacific basin during wintertime", *J. Geophys. Res., 102*, 28203-28313, 1997.

Talbot, R.W., J.E. Dibb, E.M. Scheuer, D.R. Blake, N.J. Blake, G.L. Gregory, G.W. Sachse, J.D. Bradshaw, S.T. Sandholm, and H.B. Singh, "Influence of biomass combustion emissions on the distribution of acidic trace gases over the southern Pacific basin during austral springtime", *J. Geophys. Res.*, *104*, 5623-5634, 1999.

Talbot, R., J. Dibb, E. Scheuer, G. Seid, R. Russo, S. Sandholm, D. Tan, H. Singh, D. Blake, N. Blake, E. Atlas, G. Sachse, and M. Avery, "Reactive nitrogen in Asian continental outflow over the western Pacific: results from the NASA TRACE-P Airborne mission", submitted to the TRACE-P special issue, *J. Geophys. Res.*

Tang, I.N., and H.R. Munkelwitz, "Determination of vapor pressure from droplet evaporation kinetics", *J. Coll. and Int. Sci., 141*, 109-118, 1991.

Tanner, D.J., and F.L. Eisele, "Present OH measurement limits and uncertainties", *J. Geophys. Res., 100*, 2883-2892, 1995.

Underwood, G.M., C.H. Song, M. Phadnis, G.R. Carmichael, and V.H. Grassian, "Heterogeneous reactions of NO_2 and HNO_3 on oxides and mineral dust: a combined laboratory and modeling study", *J. Geophys. Res.*, *106*, 18055-18066, 2001.

Weber, R.J., D. Orsini, Y. Daun, Y.-N. Lee, P.J. Klotz, and F. Brechtel, "A particle-into-liquid collector for rapid measurement of aerosol bulk chemical composition", *Aerosol Sci. Tech., 35,* 718-727, 2001.

Zondlo, M.A., S.B. Barone, and M.A. Tolbert, "Uptake of HNO_3 on ice under upper tropospheric conditions", *Geophys. Res. Lett., 24*, 1391-1394, 1997.

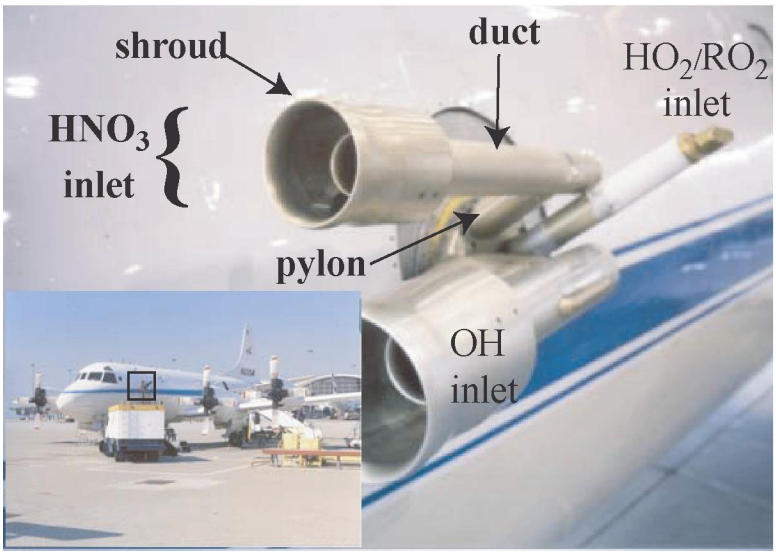

Figure 1. Photograph of the HNO_3 inlet showing the shroud, duct, and pylon. Also marked are the OH/H_2SO_4/MSA inlet as well as the HO_2/RO_2 inlet. The inlets are located on the front, port side of the P-3B aircraft shown in the box in the lower left inset.

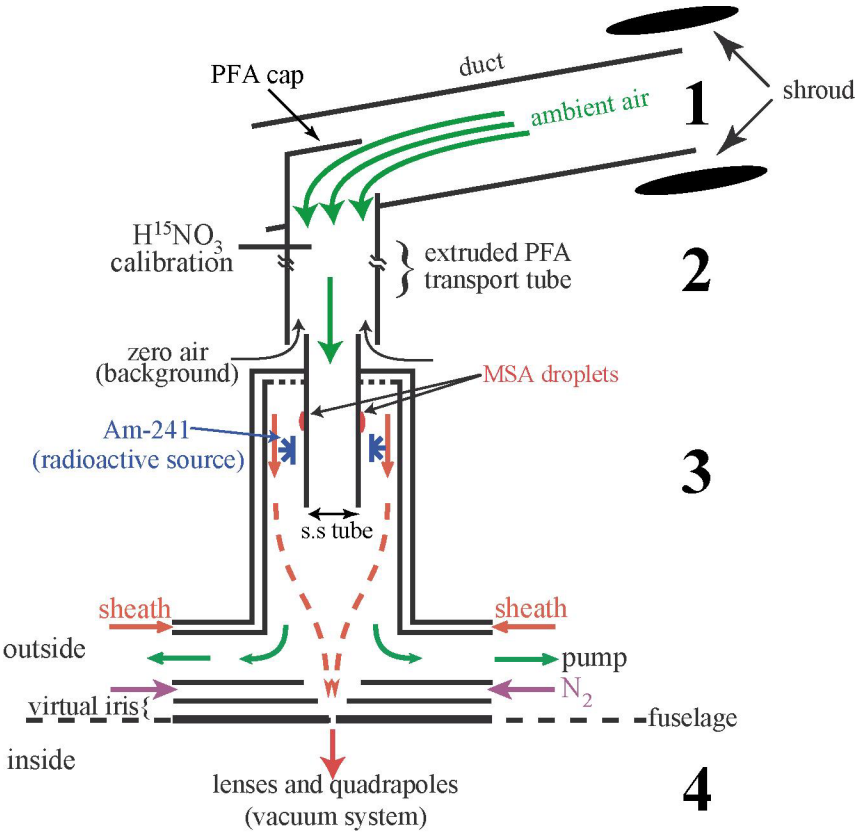

Figure 2. Schematic of the inlet and ion source showing the duct (1), transport tube (2), ion source (3), and vacuum system (4). A sample of ambient air is pulled toward the extruded PFA transport tube where isotopically-labeled 15-N nitric acid is added for calibration. The ambient air continues through a stainless steel tube into the ion source where ion-molecule reactions occur. MSA ions are generated when the sheath flow of zero air draws the vapor off tiny MSA droplets and passes over the Am-241 foil. Ions meet the ambient air and are then directed through a flow of dry nitrogen before entering the virtual iris and finally the vacuum system. Backgrounds were determined by flowing zero air immediately above the ion source and by removing the flow of the calibration gas.

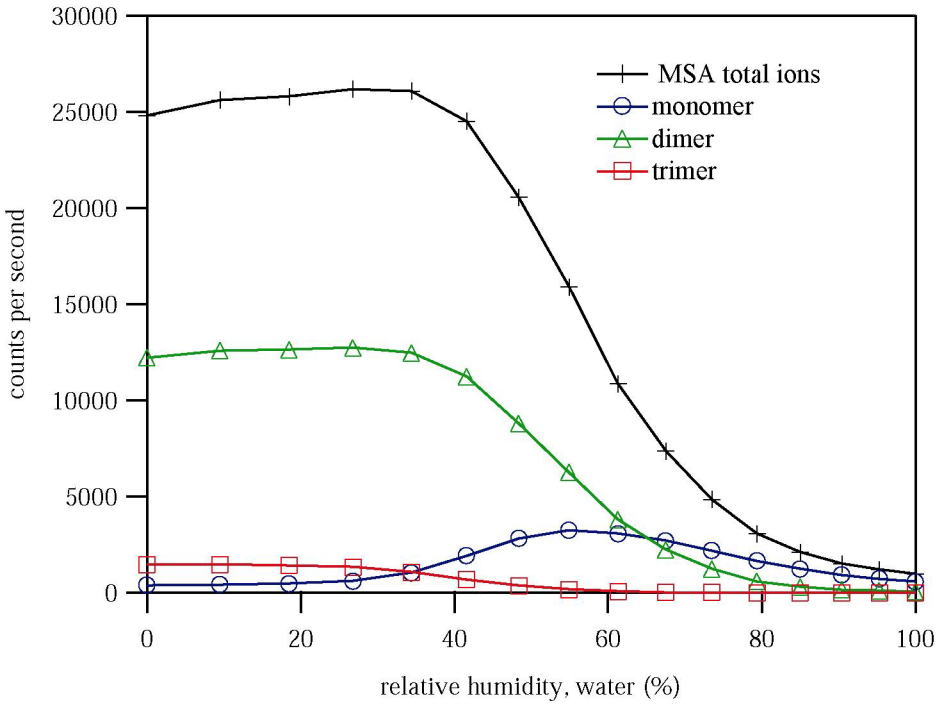

Figure 3. Plot of the populations of monomer (○, m/e=95), dimer (Δ, m/e 191), and trimer (□, m/e 287) clusters of MSA ions as a function of relative humidity at 23°C. The total number of MSA species detected (+, = 3*trimer+2*dimer+monomer) decreases dramatically as the humidity increases, while the dominant cluster size shifts towards the monomer.

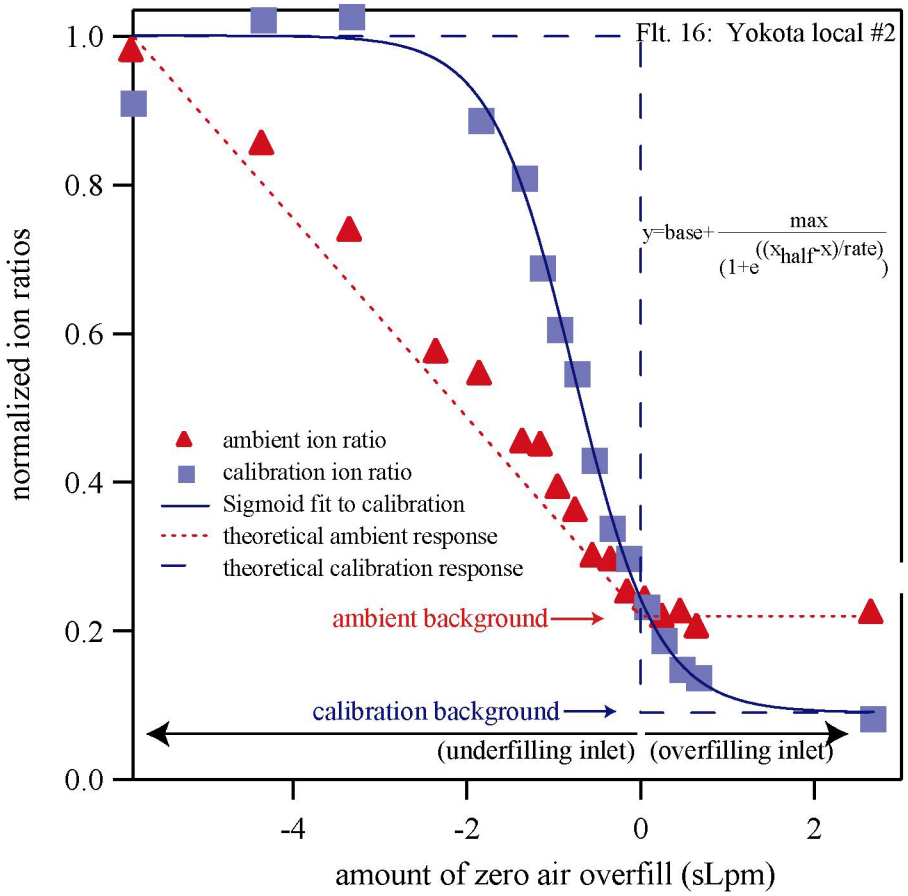

Figure 4. Response of the ambient and calibration signals upon adding a flow of zero air directly above the ion source from 5:13-5:31 UT on Flight 16 at an airspeed of 297 knots at 674 mb. The mean ambient mixing ratio was 83 pptv and the mean calibration mixing ratio was 245 pptv. The equivalence point of 0 sLpm is where the flow into the ion source equals the flow of zero air above it. Neglecting turbulence, the expected responses of the ambient and calibration signals are shown as dashed lines. Both signals were normalized to unity for comparison purposes. Fit parameters for the calibration (±1s): base = 1.00±0.02, max = -0.91 ±0.04, xhalf = -0.77±0.05, rate = 0.48±0.05.

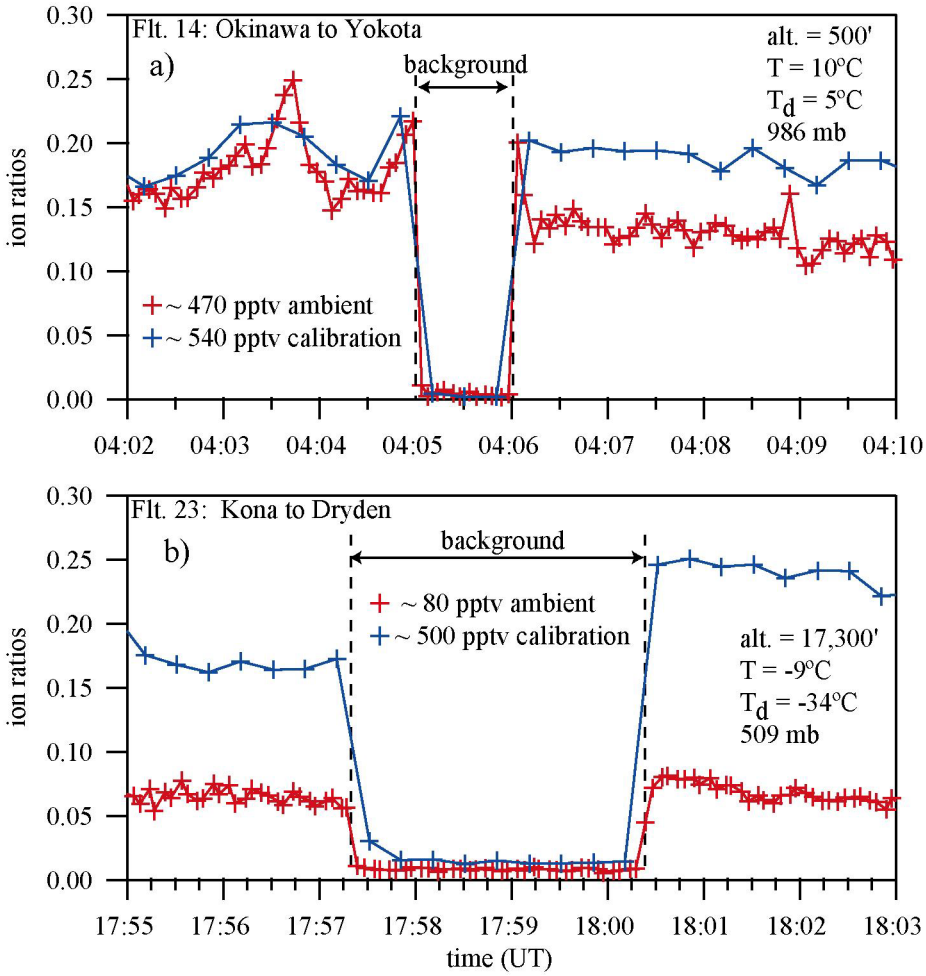

Figure 5. The response of the ambient (5 s resolution) and calibration signals (20 s resolution) upon flowing zero air in front of the ion source: (a) 500' on Flight 14 and (b) 17,300' on Flight 23. Background signals were attained within the 5 s resolution of the measurements.

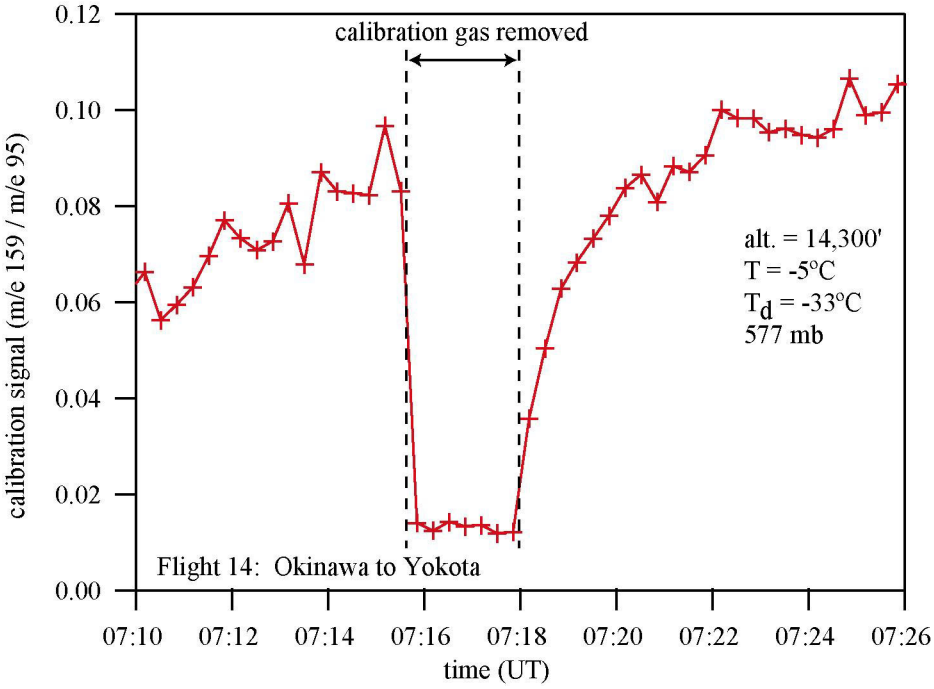

Figure 6. Response of the calibration signal when a flow of 515 pptv $H^{15}NO_3$ is removed from the inlet. A rapid (< 20s) drop to a constant, background value is observed. The gradual recovery of the signal results from re-equilibration of the $H^{15}NO_3$ concentration within the carrier flow tubing.

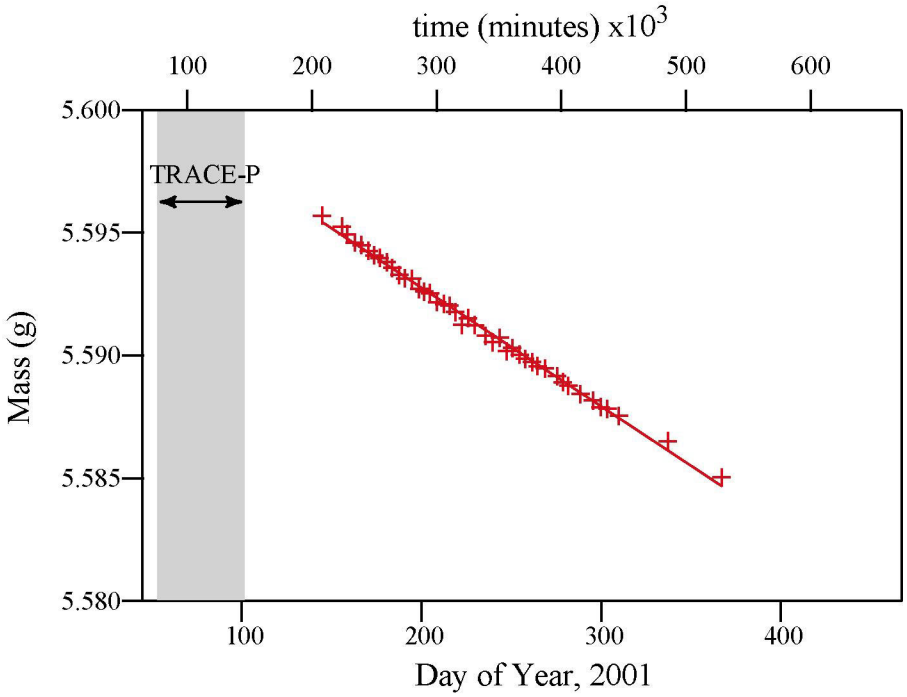

Figure 7. A plot of the mass of the $H^{15}NO_3$ permeation tube as a function of time. A linear regression of the data (±2σ) yielded a slope of -33.5 ±1.3 ng min^{-1} and an intercept of 5.6024 ± 0.0004 g for a 7+ month period after TRACE-P.

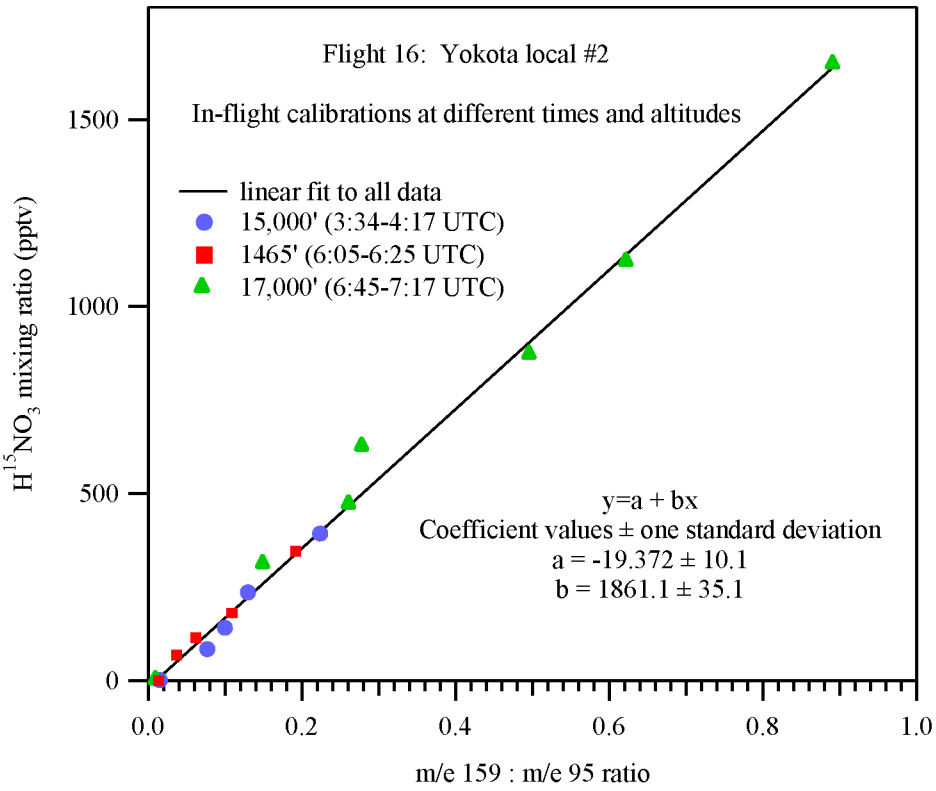

Figure 8. Plot of in-flight calibrations taken at multiple altitudes during Flight 16. The calibrations were conducted at constant altitude legs by adjusting the dilution of calibration gas.

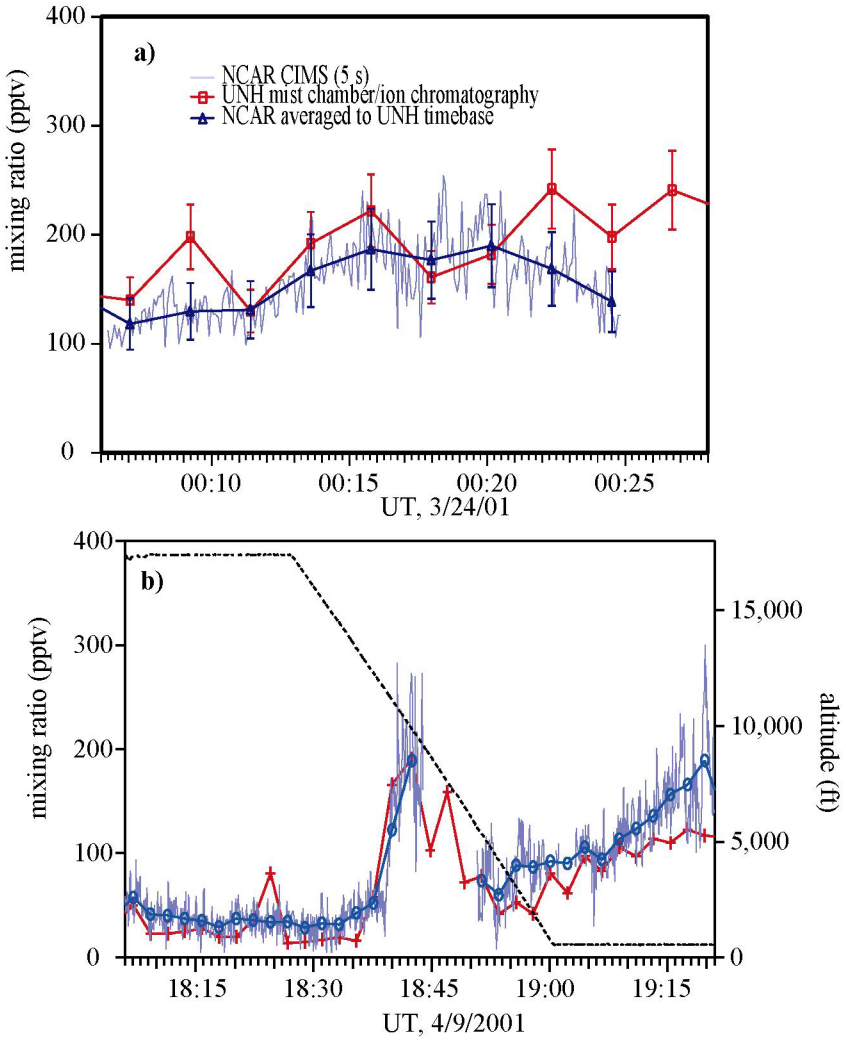

Figure 9. Results of the informal intercomparisons for HNO_3 on (a) DC-8 flight #10 and P-3B flight #16 at 17,000' off the Japan coast as well as (b) DC-8 flight #20 and P-3B flight #23 at a range of altitudes just east of Hawaii. The light blue, thin lines are the 5 s data obtained from the NCAR CIMS instrument. The red crosses are the HNO_3 mixing ratios measured on the DC-8 from the UNH mist chamber/ion chromatograph instrument. The dark blue circles are the NCAR data averaged over the UNH time base.

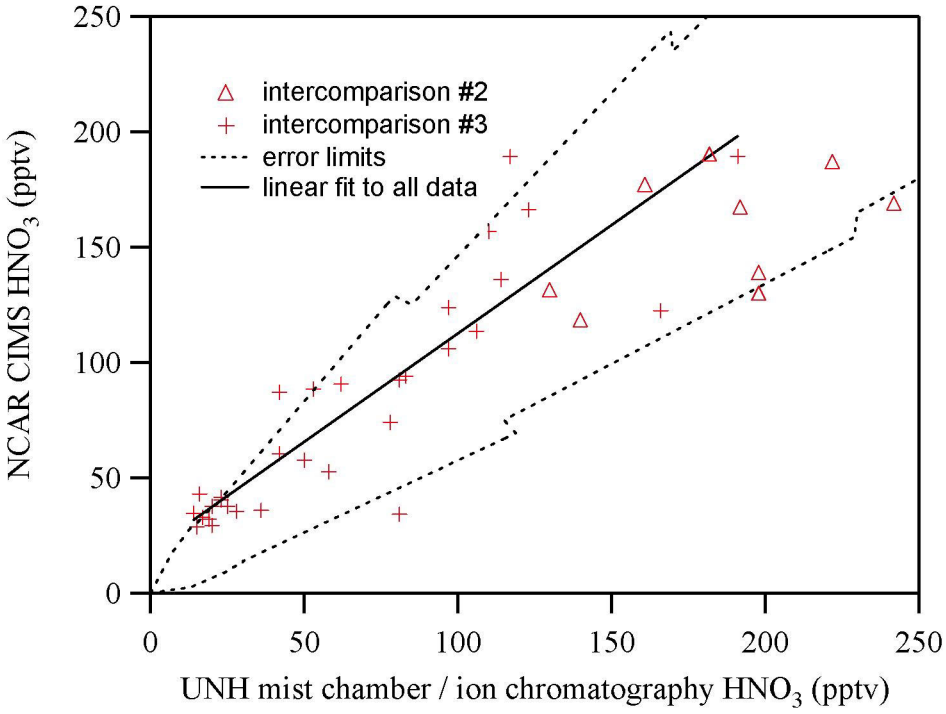

Figure 10. A plot of NCAR HNO_3 vs. UNH HNO_3 for the intercomparison flights. Triangles show intercomparison #2 while crosses mark intercomparison #3. A linear fit to the data yields an intercept of 19 ± 14 and a slope of 0.94 ± 0.18 (2σ). Dashed lines show the error limits of the two measurement.

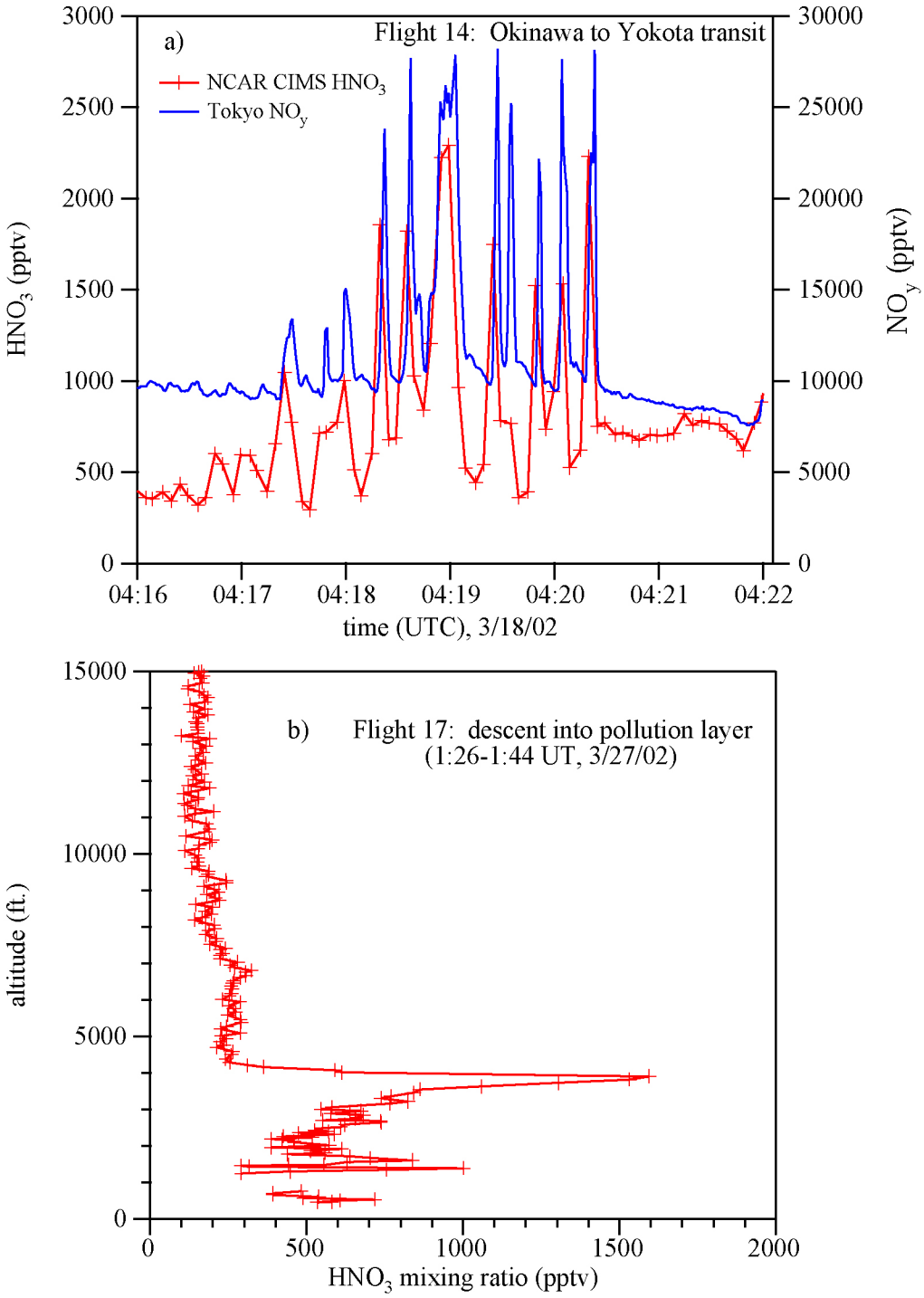

Figure 11. Rapid changes in ambient HNO_3 were observed during TRACE-P, suggesting that inlet adsorption problems were not significantly affecting the measurements. a) Ship plumes over the South China Sea at 500' showing rapid variations on the 5 s measurement time b) Descent into pollution southeast of Japan showing a greater than 1200 pptv increase in 15 s.